

# Fast holonomic quantum computation on superconducting circuits with optimal control

Sai Li, Tao Chen, and Zheng-Yuan Xue\*

*Guangdong Provincial Key Laboratory of Quantum Engineering and Quantum Materials, GPETR Center for Quantum Precision Measurement, and SPTE, South China Normal University, Guangzhou 510006, China*

(Dated: December 15, 2024)

The phase factor plays a vital role in modern quantum physics. Especially, geometric phases induced in quantum evolutions have the built-in noise-resilient character, and thus found comprehensive applications in many robust quantum manipulation tasks. Here, we propose a fast scheme to construct universal quantum gates on superconducting circuits with non-Abelian geometric phases using resonant interaction of three-level quantum systems. As the evolution state always fulfill the Schrödinger equation of the govern Hamiltonian, during the cyclic quantum evolution, there will be no nonadiabatic transitions from the evolution state to other states, i.e., the orthogonal states of the evolution state. Meanwhile, arbitrary single-qubit quantum gates can be implemented in a single-loop scenario by shaping both the amplitudes and phases of two microwave fields, resonantly coupled to a transmon qubit. Moreover, nontrivial two-qubit gates can also be realized with an auxiliary transmon simultaneously coupled to the two target transmons in an effective resonant way. In particular, our proposal can be compatible to various optimal control techniques, which further enhances the robustness of the quantum operations. Therefore, our proposal represents a promising way towards fault-tolerant quantum computation on solid-state quantum circuits.

## I. INTRODUCTION

For physical realization of quantum computation, high-fidelity quantum gates are essential, and thus constructing noise-resistant quantum operation is one of the key ingredients. Meanwhile, geometric phases [1–3], determined by the global properties of the evolution paths, possess a kind of built-in noise-resilience feature against certain types of local noises [4–7]. Therefore, for large-scale quantum systems, where control lines/devices will inevitably cause different local noises, it is more promising to realize quantum manipulations in a geometric strategy [8]. Furthermore, based on the intrinsic noncommutativity of the non-Abelian geometric phases [2], it can naturally be used to construct universal set of quantum gates, i.e., the holonomic quantum computation (HQC) [9].

Due to the limited coherent time of quantum system, the physical realization of HQC based on fast nonadiabatic evolution [3, 10, 11] is highly desirable. Recently, nonadiabatic HQC (NHQC) based on three-level systems have achieved significant theoretical [12–32] and experimental progress [33–45]. However, this type of NHQC implementation is sensitive to the systematic error [46–48].

Here, we propose a fast scheme to construct universal holonomic quantum gates on superconducting circuits [49–51], where the systematic error can be greatly suppressed. In our scheme, each transmon device [52] serves as a qubit and we only use resonant sequential transitions [53], driven by two microwave fields, of the ladder type three levels in a transmon qubit. Meanwhile, during the cyclic quantum evolution, the evolution state always fulfill the Schrödinger equation of the govern Hamiltonian [54], i.e., no nonadiabatic transitions from the evolution state to its orthogonal states will occur. In addition, at the end of the cyclic evolution, the pure geometric phase can be acquired after cancelling the dynamical

phase, thus the proposed gates are of the geometric nature. In this way, arbitrary single-qubit quantum gates can be implemented in a single-loop scenario by shaping both the amplitudes and phases of two microwave fields. Moreover, nontrivial two-qubit gates can be realized with an auxiliary transmon simultaneously coupled to the two target transmons in an effective resonant way, similar to Ref. [55]. In particular, our proposal can be compatible to various optimal control techniques [54, 56], which further enhances the robustness of the quantum operations.

## II. UNIVERSAL SINGLE-QUBIT GATES

We now proceed to present our scheme based on superconducting circuits via inverse engineering the Schrödinger equation. Firstly, arbitrary single-qubit gates can be implemented by using two resonant driving microwave fields with time dependent amplitudes and phases. Then, we show that our scheme is compatible with optimal control methods, thus the robustness of our implementation can be further improved.

### A. Inverse engineering of Hamiltonian

In this section, we introduce how to inversely engineer the Hamiltonian based on the Schrödinger equation on superconducting circuits. In a superconducting transmon device, we consider the three lowest levels  $|g\rangle$ ,  $|e\rangle$  and  $|f\rangle$ , with  $|g\rangle$ ,  $|f\rangle$  being our qubit states and  $|e\rangle$  being an auxiliary state, to construct geometric manipulation of the device. As shown in Fig. 1(a), two microwave fields  $\Omega_j(t) \cos(\omega_j t + \phi_j(t))$  ( $j = 1, 2$ ), with  $\Omega_j(t)$ ,  $\omega_j$  and  $\phi_j(t)$  being the amplitudes, frequencies and phases, resonantly coupled to the sequential transitions of the three lowest levels of a transmon. Ignoring the higher order oscillating terms, the effective interaction Hamiltonian

\* zyxue83@163.com

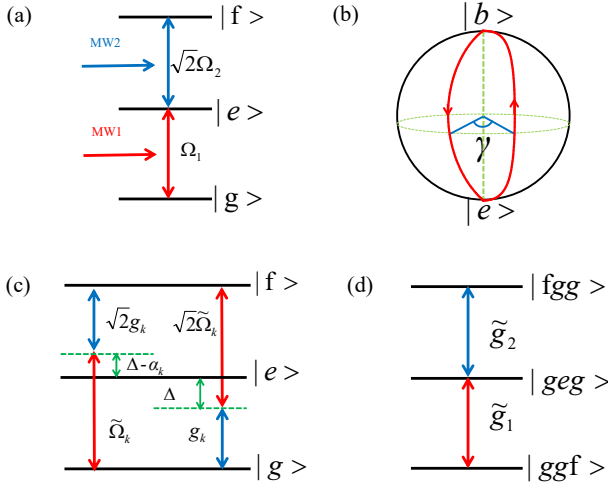


FIG. 1. Illustration of the proposal. (a) The three-level configuration of the resonant situation for the single-qubit gates, with two microwave fields resonantly coupled to the three levels of a transmon qubit respectively. (b) Geometric diagram of the proposed single-qubit gate. (c) Effective resonant qubit-qubit coupling configuration induced by two driving qubits coupled to an auxiliary transmon for non-trivial two qubit gates. (d) The effective coupling configuration for two-qubit gate in the single-excitation subspace.

can be written as

$$H_1 = \left[ \frac{\Omega_1(t)}{2} e^{i\phi_1(t)} |g\rangle + \frac{\Omega_2(t)}{\sqrt{2}} e^{-i\phi_2(t)} |f\rangle \right] \langle e| + \text{H.c.} \\ = \Omega e^{i\phi_1(t)} |b\rangle \langle e| + \text{H.c.}, \quad (1)$$

where  $\Omega = \sqrt{(\frac{\Omega_1(t)}{2})^2 + (\frac{\Omega_2(t)}{\sqrt{2}})^2}$ ,  $|b\rangle = \sin(\theta/2)|g\rangle - \cos(\theta/2)e^{-i\phi}|f\rangle$  with  $\tan(\theta/2) = \frac{\Omega_1}{\sqrt{2}\Omega_2}$  and  $\phi = \phi_2(t) + \phi_1(t) + \pi$  being time independent, and dark state  $|d\rangle = -\cos(\theta/2)e^{i\phi}|g\rangle - \sin(\theta/2)|f\rangle$  is decoupled.

Assuming  $\hbar = 1$  hereafter, Hamiltonian  $H_1$  satisfies the Schrödinger equation of

$$i \frac{\partial}{\partial t} |\Psi(t)\rangle = H_1(t) |\Psi(t)\rangle, \quad (2)$$

where the eigenstate  $|\Psi(t)\rangle$  can generally be parameterized by using two angles  $\chi, \varphi$  and with a global phase  $f$  as

$$|\Psi(t)\rangle = e^{-if/2} \begin{pmatrix} \cos \frac{\chi}{2} e^{-i\varphi/2} \\ \sin \frac{\chi}{2} e^{i\varphi/2} \end{pmatrix}. \quad (3)$$

Inserting  $|\Psi(t)\rangle$  into the Schrödinger equation, we get

$$\dot{\chi} = -2\Omega \sin(\phi_1 + \varphi), \quad (4a)$$

$$\dot{\varphi} = -2\Omega \cot \chi \cos(\phi_1 + \varphi), \quad (4b)$$

$$\dot{f} = -\dot{\varphi} / \cos \chi. \quad (4c)$$

That is to say, if the parameters of the driving microwave fields satisfy the above relations, the state  $|\Psi(t)\rangle$  will be a time dependent eigenstate of Hamiltonian  $H_1(t)$  [54], i.e., no transitions from the state  $|\Psi(t)\rangle$  to its orthogonal states will occur during the quantum evolution governed by Hamiltonian  $H_1(t)$ .

## B. Gate implementation

Now, we proceed to implement arbitrary holonomic single-qubit gates. A set of proper parameters  $\chi$  and  $\varphi$  is chosen to realize a certain evolution and once the parameters  $\chi$  and  $\varphi$  are set, the corresponding  $\Omega$  and  $\phi_1$  can be obtained by solving the Eq. (4), i.e.,

$$\phi_1 = \arctan\left(\frac{\dot{\chi}}{\dot{\varphi}} \cot \chi\right) - \varphi, \quad (5) \\ \Omega = -\frac{\dot{\chi}}{2 \sin(\phi_1 + \varphi)},$$

and thus fix the Hamiltonian in  $H_1(t)$ . Here, we consider inducing a pure geometric phase for quantum computation purpose from a cyclic evolution, which can be achieved by setting  $\chi(0) = \chi(\tau) = 0$  in Eq. (3), i.e., the state will start from  $|b\rangle$  state and go back to it after an periodical evolution with time  $\tau$ , only acquiring a phase factor. During the process, the phase factor may consist of both the geometric and the dynamical ones, and the dynamical phase is calculated to be

$$\gamma_d(\tau) = -\int_0^\tau \langle \Psi(t) | H_1 | \Psi(t) \rangle dt = \int_0^\tau \frac{\dot{\chi} \sin^2 \chi}{2 \cos \chi} dt. \quad (6)$$

In order to induce a pure geometric phase, the dynamical phase should be zero at the end of the cyclic evolution, i.e.,  $\gamma_d(\tau) = 0$ .

In the following, we adopt a single-loop evolution path, as illustrated in Fig. 1(b), to induce a pure geometric phase that can be used to achieve universal single-qubit gates. Specifically, the evolution path is divided into two equal parts, in the first path  $t \in [0, \tau/2]$ , we set

$$\chi_1 = \pi \sin^2 \left( \frac{\pi t}{\tau} \right), \quad (7) \\ \varphi_1 = -\frac{\pi}{5} \sin \left( \frac{2\pi t}{\tau} \right) - \frac{\pi}{2},$$

the corresponding evolution operator is  $U_1 = |d\rangle \langle d| + e^{i\gamma_1} |e\rangle \langle b| + e^{-i\gamma_1} |b\rangle \langle e|$ . In the second path  $t \in [\tau/2, \tau]$ , we choose

$$\chi_2 = \pi \sin^2 \left( \frac{\pi t}{\tau} \right), \quad (8) \\ \varphi_2 = \frac{\pi}{5} \sin \left( \frac{2\pi t}{\tau} \right) - \gamma - \frac{\pi}{2},$$

where  $\gamma$  is an arbitrary constant angle. The corresponding evolution operator is  $U_2 = |d\rangle \langle d| + e^{i\gamma_2} |b\rangle \langle e| + e^{-i\gamma_2} |e\rangle \langle b|$ . Then, the final evolution operator can be obtained as

$$U(\tau) = U_2 U_1 = |d\rangle \langle d| + e^{i\gamma} |b\rangle \langle b| = e^{i\frac{\gamma}{2}} e^{-i\frac{\gamma}{2} \mathbf{n} \cdot \boldsymbol{\sigma}} \quad (9)$$

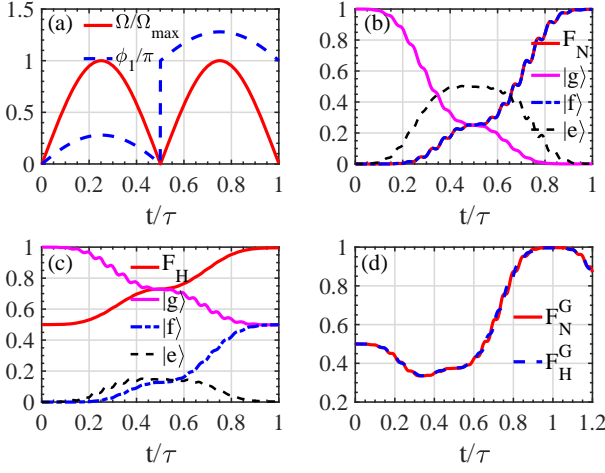


FIG. 2. (a) The parameter shapes of the Hamiltonian  $H_1(t)$ . (b) and (c) successively describe the state population and fidelity dynamics of the NOT gate and the Hadamard gate. (d) The gate fidelity dynamics of NOT gate and Hadamard gate.

where  $\gamma = \gamma_1 + \gamma_2$ ,  $\mathbf{n} = (\sin \theta \cos \phi, -\sin \theta \sin \phi, \cos \theta)$ ,  $\sigma$  are Pauli matrices. The evolution operator is a rotation operator around the axis  $\mathbf{n}$  by an angle  $\gamma$ , can be used to generate arbitrary single-qubit gates in qubit subspace in a holonomic way. Especially, we note that when  $\dot{\phi}$  or  $\dot{f}$  is zero, i.e.,  $\chi = \pi \sin^2(\pi t/\tau)$  but  $\phi_{1,2}$  are constant, our scheme reduce to the previous NHQC one.

The performance of the single-qubit gate can be evaluated by the Lindblad master equation of

$$\dot{\rho}_1 = i[\rho_1, H_1] + \frac{1}{2} [\Gamma_1 \mathcal{L}(\sigma_1) + \Gamma_2 \mathcal{L}(\sigma_2)], \quad (10)$$

where  $\rho_1$  is the density matrix of the considered system and  $\mathcal{L}(\mathcal{A}) = 2\mathcal{A}\rho_1\mathcal{A}^\dagger - \mathcal{A}^\dagger\mathcal{A}\rho_1 - \rho_1\mathcal{A}^\dagger\mathcal{A}$  is the Lindbladian of the operator  $\mathcal{A}$ ,  $\sigma_1 = |g\rangle\langle e| + \sqrt{2}|e\rangle\langle f| + \sqrt{3}|f\rangle\langle h|$ ,  $\sigma_2 = |e\rangle\langle e| + 2|f\rangle\langle f| + 3|h\rangle\langle h|$  with  $\Gamma_1$  and  $\Gamma_2$  being the corresponding decay and dephasing rates. Here, we consider the case  $\Gamma_1 = \Gamma_2 = 2\pi \times 5$  kHz [57], corresponding to a coherent time of 32  $\mu$ s, which is well accessible with current technologies. The anharmonicity of the transmon is set to be  $\alpha = \omega_{ge} - \omega_{ef} = 2\pi \times 400$  MHz [55]. Assuming the initial state  $|\psi_1\rangle = |g\rangle$  and  $\tau \simeq 51$  ns, the shapes of  $\Omega$  and  $\phi_1$  are shown in Fig. 2(a) with  $\Omega_{max} = 2\pi \times 16$  MHz. Note that there will be a bounded maximum amplitude due to the limited anharmonicity of the transmon device. Then, the NOT gate with  $\theta = \pi/2$ ,  $\phi = 0$ ,  $\gamma = \pi$  and the Hadamard gate with  $\theta = \pi/4$ ,  $\phi = 0$ ,  $\gamma = \pi$  are evaluated, using the state fidelity defined by  $F_{N/H} = {}_{N/H} \langle \psi_f | \rho_1 | \psi_f \rangle_{N/H}$  with  $|\psi_f\rangle_N = |f\rangle$  and  $|\psi_f\rangle_H = (|g\rangle + |f\rangle)/\sqrt{2}$  being the corresponding target state. The obtained fidelities are as high as  $F_N = 99.79\%$  and  $F_H = 99.55\%$ , as shown in Fig. 2(b) and Fig. 2(c), respectively. The infidelity is mainly due to both the leakage caused by the small anharmonicity and relaxation and dephasing of the qubits and auxiliary state  $|e\rangle$ . In addition, for a general initial state  $|\psi_1\rangle = \cos \theta' |g\rangle + \sin \theta' |f\rangle$ , the

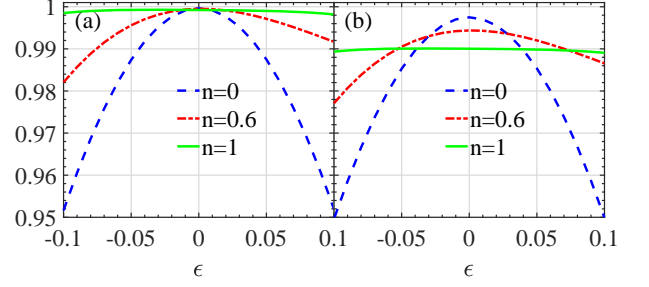


FIG. 3. (a) and (b) exhibit the gate fidelity dynamics of NOT gate with different values  $n$  under the systematic error  $-0.1 \leq \epsilon \leq 0.1$  without and with the decoherence, respectively.

NOT and Hadamard gates should result in an ideal final state  $|\psi_f\rangle_N = \sin \theta' |g\rangle + \cos \theta' |f\rangle$  and  $|\psi_f\rangle_H = \frac{1}{\sqrt{2}}[(\cos \theta' + \sin \theta')|g\rangle + (\cos \theta' - \sin \theta')|f\rangle]$ . To fully evaluate the performance of the implemented gates, we define the gate fidelity as  $F_{N/H}^G = (\frac{1}{2\pi}) \int_0^{2\pi} {}_{N/H} \langle \psi_f | \rho_1 | \psi_f \rangle_{N/H} d\theta'$  [58] with the integration numerically performed for 1001 input states with  $\theta'$  being uniformly distributed over  $[0, 2\pi]$ . In Fig. 2(d), we have plotted the gate fidelities, where we find that the gate fidelities are  $F_N^G = 99.75\%$  and  $F_H^G = 99.62\%$ .

### C. Optimal Control

Due to the parametric constrain, the previous NHQC implementations are sensitive to the systematic error [46, 47]. Meanwhile, it is difficult to incorporate optimal control technique without additional adjustable parameters. Here, as our scheme introduce additional time dependent phase factors, we can adopt 'zero systematic-error sensitivity'-optimal protocol [56] to further suppress the sensitive of our implementation to the systematic error. To begin with, we consider the static systematic error situation, i.e.  $\Omega \rightarrow (1 + \epsilon)\Omega$ . Therefore, the Hamiltonian can be written as

$$H_\epsilon(t) = (1 + \epsilon)\Omega e^{i\phi_1} |b\rangle\langle e| + \text{H.c.}, \quad (11)$$

In our implementation, at the end of the first interval  $\tau/2$ , to evaluate the influence of the static systematic error, the excitation profile is given as

$$P = |\langle \Psi(\tau/2) | \Psi_\epsilon(\tau/2) \rangle|^2 = 1 + \tilde{O}_1 + \tilde{O}_2 + \dots, \quad (12)$$

where  $|\Psi_\epsilon(\tau/2)\rangle$  is the state with the static systematic error, and  $\tilde{O}_m$  is the perturbation term of order  $m$ . Here, we only consider the excitation profile  $P$  to the second order, i.e.,  $P_2 = 1 - \epsilon^2 q_s$ , where

$$q_s = -\frac{\partial P_2}{\partial(\epsilon^2)} = \left| \int_0^{\tau/2} e^{-if} \dot{\chi} \sin^2 \chi dt \right|^2 \quad (13)$$

represents the systematic error sensitivity. To nullify the  $q_s$ , we set  $f(\chi) = n[2\chi - \sin(2\chi)]$ ,  $\varphi_1(0) = 0$  and  $\varphi_2(\tau/2) =$

$-\gamma$ , which lead to  $q_s = \sin^2 n\pi/(2n)^2$ , i.e., for positive integer  $n$ ,  $q_s = 0$ . When  $n \rightarrow 0$ ,  $q_s \rightarrow \pi^2/4$ , the current implementation reduces to the previous NHQC case. In the following numerical simulations, all the  $\Omega$  are set to be  $\Omega_{max} = 2\pi \times 16$  MHz as a restriction. That is the maximum value of the optimized pulse is bounded by  $\Omega_{max}$ , and thus the improvement of the gate performance can only be attributed to the optimal control.

However, in the case of  $n \geq 1$ , under the restriction, the evolution time  $\tau$  will too long, and decoherence will introduce unacceptable gate infidelity. Therefore, we need to confirm the optimal value of  $n$  under the targets with both short time  $\tau$  and low systematic error sensitivity. To find out the optimal value  $n$  under decoherence, we simulated the NOT gate fidelity under the systematic error  $-0.1 \leq \epsilon \leq 0.1$  while changing  $n$  from 0 to 1 with the uniform step  $dn = 0.1$ . In this way, we find out that  $n = 0.6$  is an optimal value. In Fig. 3(a) and 3(b), we plot the gate fidelity in the case  $n = 1$ ,  $n = 0.6$ ,  $n = 0$  without and with decoherence, respectively. From the Fig. 3(a), we find out that the robustness of the holonomic quantum gates is significant improved comparing  $n = 1$  with  $n = 0$ , corresponding to the previous NHQC scheme. From Fig. 3(b), considering the decoherence effect, we find that  $n = 0.6$  will be better. Therefore, for the long coherence time quantum systems, our scheme will significantly improve the robustness of the holonomic quantum gates.

### III. NONTRIVIAL TWO-QUBIT GATES

In this section, we proceed to implement nontrivial two-qubit quantum gates. Based on the current experimental technique, the strong capacity coupling between transmon qubits has been achieved experimentally on superconducting circuits [59–61]. Here, we consider the case that the two driving transmon qubits are capacitively coupled simultaneously to an auxiliary transmon by the capacity coupling. As shown in Fig. 1(c), the auxiliary transmon with frequency  $\omega_A$  dispersively coupled to both qubits with frequencies  $\omega_{ge}^k$  ( $k = 1, 2$ ). Meanwhile, the sequential transitions of both qubits are driving by microwave field with time dependent driving amplitude  $\tilde{\Omega}_k(t)$ , frequency  $\tilde{\omega}_k(t)$  and phase  $\tilde{\phi}_k(t)$ . In the rotating framework with respect to the driving frequency, the Hamiltonian of the  $k$ th qubit coupled to the auxiliary transmon can be written as

$$H_0 = \delta_k N_k + \delta_A N_A - \frac{\alpha_k}{2} (N_k - 1) N_k - \frac{\alpha_A}{2} (N_A - 1) N_A$$

$$H' = g_k a b_k^\dagger + \frac{\tilde{\Omega}_k e^{i\tilde{\phi}_k}}{2} b_k + \text{H.c.}, \quad (14)$$

where  $\delta_k = \omega_{ge}^k - \tilde{\omega}_k$ ,  $\delta_A = \omega_A - \tilde{\omega}_k$ , and  $N_A = a^\dagger a$ ,  $N_k = b_k^\dagger b_k$ , with  $a = |g\rangle_A \langle e| + \sqrt{2}|e\rangle_A \langle f| + \sqrt{3}|f\rangle_A \langle h| + \dots$ ,  $b_k = |g\rangle_k \langle e| + \sqrt{2}|e\rangle_k \langle f| + \sqrt{3}|f\rangle_k \langle h| + \dots$  being the lower operator for the auxiliary transmon and the qubits. As all the sequential transitions are allowed in both qubits, the effective interaction will be generated from the interference of the two paths. In addition, the two couplings form a two-photon resonant situation, i.e.,  $\omega_{ge}^k - \omega_A = \tilde{\omega}_k - \omega_{fe}^k = \Delta > \alpha_k$ , and

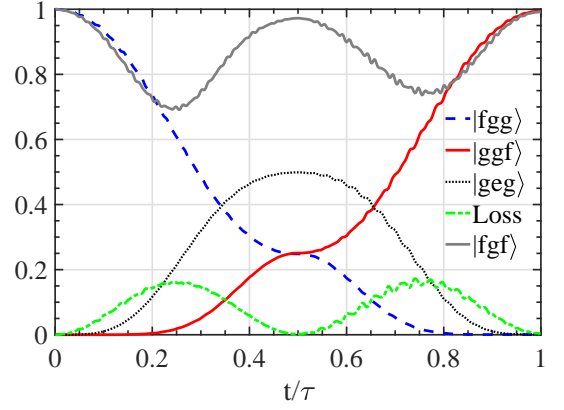


FIG. 4. State population and fidelity dynamics for gate as a function of time with the initial state being  $|fgg\rangle$  with Loss and initial state being  $|fgf\rangle$ .

thus lead to driving-assisted coherent resonant coupling between the auxiliary transmon and the  $|g\rangle_k \leftrightarrow |f\rangle_k$  transition of the qubits (see Appendix A for details), the Hamiltonian may be expressed as

$$\tilde{H}_2 = \eta_{ge} |g, e\rangle_{k,A} \langle g, e| + \eta_{fg} |f, g\rangle_{k,A} \langle f, g|$$

$$+ \left( \tilde{g}_k e^{-i\tilde{\phi}_k} |f, g\rangle_{k,A} \langle g, e| + \text{H.c.} \right), \quad (15)$$

where

$$\eta_{g1} = \frac{\tilde{\Omega}_k^2}{4(\Delta - \alpha_k)} - \frac{g_k^2}{\Delta}$$

$$\eta_{f0} = \frac{3\tilde{\Omega}_k^2}{4(\Delta + \alpha_k)} + \frac{2g_k^2}{\Delta - \alpha_k} - \frac{\tilde{\Omega}_k^2}{2\Delta} \quad (16)$$

$$\tilde{g}_k = \frac{\sqrt{2}g_k\tilde{\Omega}_k}{2(\Delta - \alpha_k)} - \frac{\sqrt{2}g_k\tilde{\Omega}_k}{2\Delta} = \frac{g_k\tilde{\Omega}_k\alpha_k}{\sqrt{2}\Delta(\Delta - \alpha_k)},$$

We set  $\Delta \gg \{g_k, \tilde{\Omega}_k\}$ , after concealing the cross-ac-Stark-shifts by modulating the frequencies of the driving fields accordingly to  $\tilde{\Omega}_k$  (see Appendix B for details), in the single-excitation subspace  $S_1 = \text{span}\{|ggf\rangle, |fgg\rangle, |geg\rangle\}$ , where  $|lms\rangle \equiv |l\rangle_1 \otimes |m\rangle_A \otimes |s\rangle_2$  labels the product states of the two qubits and the auxiliary transmon, the effective interaction Hamiltonian can be described by

$$H_{eff} = \tilde{g}_1 e^{-i\tilde{\phi}_1} |fgg\rangle \langle geg| + \tilde{g}_2 e^{-i\tilde{\phi}_2} |ggf\rangle \langle geg| + \text{H.c.}$$

$$= \tilde{g} e^{-i\tilde{\phi}} |B\rangle \langle E| + \text{H.c.}, \quad (17)$$

where  $\tilde{g} = \sqrt{\tilde{g}_1^2 + \tilde{g}_2^2}$ , bright state  $|B\rangle = \sin(\vartheta/2)|fgg\rangle - e^{-i\tilde{\phi}} \cos(\vartheta/2)|ggf\rangle$  with  $\tan(\vartheta/2) = \tilde{g}_1/\tilde{g}_2$  and  $\tilde{\phi} = \tilde{\phi}_2 - \tilde{\phi}_1 + \pi$ ,  $|E\rangle = |geg\rangle$ , and dark state  $|D\rangle = -\cos(\vartheta/2)e^{i\tilde{\phi}}|fgg\rangle - \sin(\vartheta/2)|ggf\rangle$  is decoupled. The above effective Hamiltonian, which can readily be used to implement nontrivial two-qubit gates, establishes a coupled three-level Hamiltonian in the single-excitation subspace with  $|E\rangle$  being an auxiliary state, as illustrated in Fig. 1(d). Then, we can adopt the same

protocol as for the single-qubits case to implement holonomic two-qubit gates. Notably,  $\tilde{g}$  and  $\tilde{\phi}_1$  in the effective Hamiltonian in Eq. (17) can also be solved by Eq. (2) similar to the single-qubits case, i.e.

$$\begin{aligned}\tilde{\phi}_1 &= \varphi' - \arctan\left(\frac{\dot{\chi}'}{\dot{\varphi}'} \cot \chi'\right), \\ \tilde{g} &= \frac{\dot{\chi}'}{2 \sin(\tilde{\phi}_1 - \varphi')},\end{aligned}\quad (18)$$

where  $\chi'$  and  $\varphi'$  are chosen the same form in Eq. (7) and Eq. (8), after that, the effective Hamiltonian can be fixed. Thus, for the case of  $\tilde{\gamma} = \pi$ ,  $\tilde{\phi} = 0$ , the evolution operator in the two-qubit gate Hilbert space  $S_2 = \text{span}\{|gg\rangle, |gg\rangle, |fg\rangle, |ff\rangle\}$  can be written as

$$U_2(\vartheta) = \begin{pmatrix} 1 & 0 & 0 & 0 \\ 0 & \cos \vartheta & \sin \vartheta & 0 \\ 0 & \sin \vartheta & -\cos \vartheta & 0 \\ 0 & 0 & 0 & 1 \end{pmatrix}. \quad (19)$$

Now, we analyse the performance of two-qubit gates with  $\vartheta = \pi/2$ . For  $\Delta = 2\pi \times 1$  GHz, and the parameter of transmons  $g_k = 2\pi \times 65$  MHz,  $\alpha_k = 2\pi \times 400$  MHz,  $\alpha_A = 2\pi \times 370$  MHz,  $\tau_2 = 57$  ns,  $\tilde{g}_{k,max} = 10$  MHz by modulating  $\tilde{\Omega}_k(t)$  with the maximum value to be  $2\pi \times 320$  MHz. When the initial state is  $|fgg\rangle$ , a fidelity of 99.44% can be obtained, as plotted in Fig. 4. Note that, the numerical simulation is done by using the origin Hamiltonian in Eq.(14), i.e., including all the unwanted higher-order effects induced by the strong microwave driving. Similarly, the optimal control technique presented in the single-qubit implementation can also be incorporated in this two-qubit gate implementation.

#### IV. CONCLUSION

In conclusion, we have proposed and elaborated how to efficiently implement fast HQC based on capacitively coupled superconducting circuits with microwave filed driven induced effective resonant coupling. In particularly, our scheme is compatible with the optimal control technique, and thus provides a promising way towards robust HQC on superconducting circuits.

#### ACKNOWLEDGMENTS

This work was supported by the National Natural Science Foundation of China (Grant No. 11874156), the Key R&D Program of Guangdong Province (Grant No. 2018B0303326001), and the National Key R&D Program of China (Grant No. 2016 YFA0301803).

#### Appendix A: The effective Hamiltonian

Starting from the original Hamiltonian of Eq. (14) in the main text, the energies of the state  $|g, e\rangle, |f, g\rangle$  are

$$E_{f,g} = 2\delta_k - \alpha_k, \quad E_{g,e} = \delta_A, \quad (A1)$$

which can be adjusted to be degenerate by modulating  $\tilde{\omega}_k$  such that  $\delta_A = 2\delta_k - \alpha_k$ , and set  $\varepsilon = E_{f,g} = E_{g,e}$ . We then define

$$\mathcal{P} = |g, e\rangle_{k,A} \langle g, e| + |f, g\rangle_{k,A} \langle f, g|, \quad (A2)$$

$$\mathcal{K} = \sum_{\Pi} \frac{|l, m\rangle_{k,A} \langle l, m|}{\varepsilon_{l,m} - \varepsilon}, \quad (A3)$$

where the degenerate subspace  $\{|g, e\rangle_{k,A}, |f, g\rangle_{k,A}\}$  is of interest,  $\Pi : \{l, m | (l, m) \neq (g, e) \text{ or } (f, g)\}$ , and  $\varepsilon_{l,m}$  is the energy of state  $|l, m\rangle$ . In the following calculation, we only consider the fourth energy level that is beyond the qubit states.

We handle the effective Hamiltonian using a perturbation theory with  $\{g_k, \tilde{\Omega}_k\} \ll \Delta = \delta_k - \delta_A$ , the first-order term is found to be

$$\tilde{H}_1 = \mathcal{P} H' \mathcal{P} = 0, \quad (A4)$$

as

$$\begin{aligned}H' \mathcal{P} &= \left( g_k |e, g\rangle + \frac{\tilde{\Omega}_k}{2} e^{-i\tilde{\phi}_k} |e, e\rangle \right)_{k,A} \langle g, e| \\ &+ \left( \sqrt{2} g_k |e, e\rangle + \frac{\sqrt{2}\tilde{\Omega}_k}{2} e^{i\tilde{\phi}_k} |e, g\rangle \right. \\ &\left. + \frac{\sqrt{3}\tilde{\Omega}_k e^{-i\tilde{\phi}_k}}{2} |h, g\rangle \right)_{k,A} \langle f, g|. \end{aligned} \quad (A5)$$

As for the second-order terms,

$$\begin{aligned}\tilde{H}_2 &= -\mathcal{P} H' \mathcal{K} H' \mathcal{P} \\ &= -\mathcal{P} H' (\mathcal{K}_1 + \mathcal{K}_2 + \mathcal{K}_3) H' \mathcal{P},\end{aligned} \quad (A6)$$

where

$$\begin{aligned}\mathcal{K}_1 &= \frac{|e, g\rangle_{k,A} \langle e, g|}{\varepsilon_{e,g} - \varepsilon}, \\ \mathcal{K}_2 &= \frac{|e, e\rangle_{k,A} \langle e, e|}{\varepsilon_{e,e} - \varepsilon}, \\ \mathcal{K}_3 &= \frac{|h, g\rangle_{k,A} \langle h, g|}{\varepsilon_{h,g} - \varepsilon}.\end{aligned}$$

Finally, we get the Eq.(15) in main text.

#### Appendix B: Compensate of the cross-ac-Stark-shifts

In Eq. (15), there are just ac Stark shifts caused by the  $k$ th qubit coupled to an auxiliary transmon. When we consider the two qubits simultaneously coupled to an auxiliary transmon,

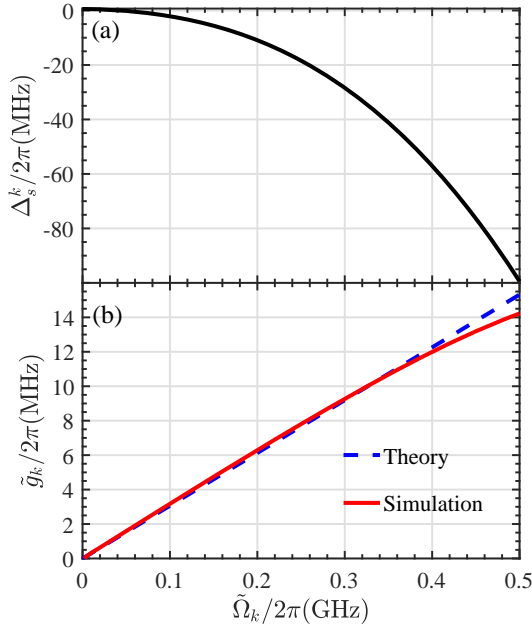


FIG. 5. (a) Illustration of the  $\Delta_s^k$  with respect to  $\tilde{\Omega}_k$  for fixed  $g_k$ . (b) Illustration of the effective transmon-transmon coupling strength  $\tilde{g}$  with respect to  $\tilde{\Omega}_k$  with fixed  $g_k$ .

the cross-ac-Stark-shifts will occur [62]. In the degenerate subspace  $S_1$ , the whole Hamiltonian can be written as

$$\begin{aligned}
 H_{\text{two}} = & \eta_{fgg}|fgg\rangle\langle fgg| + \eta_{geg}|geg\rangle\langle geg| + \eta_{ggf}|ggf\rangle\langle ggf| \\
 & + \tilde{g}_1 e^{-i\tilde{\phi}_1}|fgg\rangle\langle geg| + \left( \tilde{g}_2 e^{-i\tilde{\phi}_2}|ggf\rangle\langle geg| + \text{H.c.} \right) \\
 = & \eta_B|B\rangle\langle B| + \eta_D|D\rangle\langle D| + \eta_E|E\rangle\langle E| \\
 & + \left( \tilde{g} e^{-i\tilde{\phi}_1}|B\rangle\langle E| + \text{H.c.} \right), \quad (\text{B1})
 \end{aligned}$$

where  $\eta_{\mathcal{M}}$  is the energy level shift of the state  $|\mathcal{M}\rangle$ . Due to the existence of the cross-ac-Stark-shifts, it can lead to large errors of the gate operations. Therefore, we need to compensate these shifts. It is noted that both  $g_k$  and  $\tilde{\Omega}_k$  split the degenerate subspace  $\{|B\rangle, |D\rangle, |E\rangle\}$ , so we will fix  $g_k$  and tune the frequency  $\tilde{\omega}_k$  of the driven field to fulfill  $|\eta_B - \eta_E| = |\eta_B - \eta_D| = 0$ . However, as  $|\eta_B - \eta_E| \geq |\eta_B - \eta_D|$  due to  $\tilde{g}$ , we just need to care  $|\eta_B - \eta_E| = 0$  in the degenerate subspace  $\{|B\rangle, |E\rangle\}$ , i.e.,

$$\left\langle \phi_l(\tilde{\Omega}_k) \left| \frac{d}{d\tilde{\Omega}_k(t)} \right| \phi_m(\tilde{\Omega}_k) \right\rangle = 0.$$

Then, we obtain

$$\left\langle \phi_l(\tilde{\Omega}_k) \left| \frac{\partial H}{\partial \tilde{\Omega}_k} \right| \phi_m(\tilde{\Omega}_k) \right\rangle + \frac{d\tilde{\omega}_k}{d\tilde{\Omega}_k} \left\langle \phi_l(\tilde{\Omega}_k) \left| \frac{\partial H}{\partial \tilde{\Omega}_k} \right| \phi_m(\tilde{\Omega}_k) \right\rangle = 0,$$

which can be numerically solved to obtain the  $\tilde{\omega}_k - \tilde{\Omega}_k$  curve, such that one can figure out the  $\Delta_s^k = \tilde{\omega}_k - \tilde{\omega}_k(0)$  under the situation  $\tilde{\Omega}_1 = \tilde{\Omega}_2$  for numerical simulation, as shown in Fig. 5(a). Once the above equation is satisfied, the cross-ac-Stark-shifts must be compensated by tuning the frequency  $\tilde{\omega}_k$  of the driven field.

After that, in order to effectively conceal the cross-ac-Stark-shifts, the driven pulse with smoothly changed amplitude may be employed, which can lead to a smoothly changed effectively resonant coupling strength  $\tilde{g}_k$ . As shown in Fig. 5(b), the  $\tilde{g}_k - \tilde{\Omega}_k$  curve of the numerical simulation is coincident to the theory. Also note that when  $\tilde{\Omega}_k$  is large, the trend of  $\tilde{g}_k - \tilde{\Omega}_k$  will be slightly nonlinear.

- 
- [1] M. V. Berry, Proc. R. Soc. Lond., Ser. A **392**, 45 (1984).
  - [2] F. Wilczek and A. Zee, Phys. Rev. Lett. **52**, 2111 (1984).
  - [3] Y. Aharonov and J. Anandan, Phys. Rev. Lett. **58**, 1593 (1987).
  - [4] P. Solinas, P. Zanardi, and N. Zanghì, Phys. Rev. A **70**, 042316 (2004).
  - [5] S.-L. Zhu and P. Zanardi, Phys. Rev. A **72**, 020301(R) (2005).
  - [6] P. Solinas, M. Sassetti, T. Truini, and N. Zanghì, New J. Phys. **14**, 093006 (2012).
  - [7] M. Johansson, E. Sjöqvist, L. M. Andersson, M. Ericsson, B. Hessmo, K. Singh, and D. M. Tong, Phys. Rev. A **86**, 062322 (2012).
  - [8] E. Sjöqvist, Physics **1**, 35 (2008).
  - [9] P. Zanardi and M. Rasetti, Phys. Lett. A **264**, 94 (1999).
  - [10] W. Xiang-Bin and M. Keiji, Phys. Rev. Lett. **87**, 097901 (2001).
  - [11] S.-L. Zhu and Z. D. Wang, Phys. Rev. Lett. **89**, 097902 (2002).
  - [12] E. Sjöqvist, D. M. Tong, L. Mauritz Andersson, B. Hessmo, M. Johansson, and K. Singh, New J. Phys. **14**, 103035 (2012).
  - [13] G. F. Xu, J. Zhang, D. M. Tong, E. Sjöqvist, and L. C. Kwek, Phys. Rev. Lett. **109**, 170501 (2012).
  - [14] V. A. Mousolou and E. Sjöqvist, Phys. Rev. A **89**, 022117 (2014).
  - [15] J. Zhang, L.-C. Kwek, E. Sjöqvist, D. M. Tong, and P. Zanardi, Phys. Rev. A **89**, 042302 (2014).
  - [16] G.-F. Xu and G.-L. Long, Sci. Rep. **4**, 6814 (2014).
  - [17] G. F. Xu, C. L. Liu, P. Z. Zhao, and D. M. Tong, Phys. Rev. A **92**, 052302 (2015).
  - [18] Z.-Y. Xue, J. Zhou, and Z. D. Wang, Phys. Rev. A **92**, 022320 (2015).
  - [19] E. Sjöqvist, Phys. Lett. A **380**, 65 (2016).
  - [20] Z.-Y. Xue, J. Zhou, Y.-M. Chu, and Y. Hu, Phys. Rev. A **94**, 022331 (2016).
  - [21] P. Z. Zhao, G. F. Xu, and D. M. Tong, Phys. Rev. A **94**, 062327 (2016).
  - [22] E. Herterich and E. Sjöqvist, Phys. Rev. A **94**, 052310 (2016).
  - [23] G. F. Xu, P. Z. Zhao, T. H. Xing, E. Sjöqvist, and D. M. Tong, Phys. Rev. A **95**, 032311 (2017).
  - [24] Z.-Y. Xue, F.-L. Gu, Z.-P. Hong, Z.-H. Yang, D.-W. Zhang, Y. Hu, and J. Q. You, Phys. Rev. Appl. **7**, 054022 (2017).
  - [25] G. F. Xu, P. Z. Zhao, D. M. Tong, and E. Sjöqvist, Phys. Rev. A **95**, 052349 (2017).
  - [26] P. Z. Zhao, G. F. Xu, Q. M. Ding, E. Sjöqvist, and D. M. Tong, Phys. Rev. A **95**, 062310 (2017).



- [27] V. A. Mousolou, Phys. Rev. A **96**, 012307 (2017).
- [28] J. Zhou, B.-J. Liu, Z.-P. Hong, and Z.-Y. Xue, Sci. China: Phys. Mech. Astron. **61**, 010312 (2018).
- [29] Z.-P. Hong, B.-J. Liu, J.-Q. Cai, X.-D. Zhang, Y. Hu, Z.-D. Wang, and Z.-Y. Xue, Phys. Rev. A **97**, 022332 (2018).
- [30] G. F. Xu, D. M. Tong, and E. Sjöqvist, Phys. Rev. A **98**, 052315 (2018).
- [31] V. A. Mousolou, Phys. Rev. A **98**, 062340 (2018).
- [32] N. Ramberg and E. Sjöqvist, Phys. Rev. Lett. **122**, 140501 (2019).
- [33] A. A. Abdumalikov, J. M. Fink, K. Juliusson, M. Pechal, S. Berger, A. Wallraff, and S. Filipp, Nature (London) **496**, 482 (2013).
- [34] G. Feng, G. Xu, and G. Long, Phys. Rev. Lett. **110**, 190501 (2013).
- [35] C. Zu, W.-B. Wang, L. He, W.-G. Zhang, C.-Y. Dai, F. Wang, and L.-M. Duan, Nature (London) **514**, 72 (2014).
- [36] S. Arroyo-Camejo, A. Lazarev, S. W. Hell, and G. Balasubramanian, Nat. Commun. **5**, 4870 (2014).
- [37] Y. Sekiguchi, N. Niihara, R. Kuroiwa, H. Kano, and H. Kosaka, Nat. Photonics **11**, 309 (2017).
- [38] B. B. Zhou, P. C. Jerger, V. O. Shkolnikov, F. J. Heremans, G. Burkard, and D. D. Awschalom, Phys. Rev. Lett. **119**, 140503 (2017).
- [39] H. Li, L. Yang, and G. Long, Sci. China: Phys., Mech. Astron. **60**, 080311(2017).
- [40] Y. Xu, W. Cai, Y. Ma, X. Mu, L. Hu, T. Chen, H. Wang, Y.-P. Song, Z.-Y. Xue, Z.-Q. Yin, and L. Sun, Phys. Rev. Lett. **121**, 110501 (2018).
- [41] N. Ishida, T. Nakamura, T. Tanaka, S. Mishima, H. Kano, R. Kuroiwa, Y. Sekiguchi, and H. Kosaka, Opt. Lett. **43**, 2380 (2018).
- [42] K. Nagata, K. Kuramitani, Y. Sekiguchi, and H. Kosaka, Nat. Commun. **9**, 3227 (2018).
- [43] D. J. Egger, M. Ganzhorn, G. Salis, A. Fuhrer, P. Mueller, P. K. Barkoutsos, N. Moll, I. Tavernelli, and S. Filipp, Phys. Rev. Appl. **11**, 014017 (2019).
- [44] T. Yan, B.-J. Liu, K. Xu, C. Song, S. Liu, Z. Zhang, H. Deng, Z. Yan, H. Rong, M.-H. Yung, Y. Chen, and D. Yu, Phys. Rev. Lett. **122**, 080501 (2019).
- [45] Z. Zhu, T. Chen, X. Yang, J. Bian, Z.-Y. Xue, and X. Peng, arXiv:1902.09997 (2019).
- [46] S. B. Zheng, C. P. Yang, and F. Nori, Phys. Rev. A **93**, 032313 (2016).
- [47] J. Jing, C.-H. Lam, and L.-A. Wu, Phys. Rev. A **95**, 012334 (2017).
- [48] B.-J. Liu, X.-K. Song, Z.-Y. Xue, X. Wang, and M.-H. Yung, arXiv:1806.07904 (2018).
- [49] J. Clarke and F. K. Wilhelm, Nature (London) **453**, 1031 (2008).
- [50] J. Q. You and F. Nori, Nature (London) **474**, 589 (2011).
- [51] M. H. Devoret and R. J. Schoelkopf, Science **339**, 1169 (2013).
- [52] J. Koch, T. M. Yu, J. Gambetta, A. A. Houck, D. I. Schuster, J. Majer, A. Blais, M. H. Devoret, S. M. Girvin, and R. J. Schoelkopf, Phys. Rev. A **76**, 042319 (2007).
- [53] M. J. Peterer, S. J. Bader, X. Jin, F. Yan, A. Kamal, T. J. Gudmundsen, P. J. Leek, T. P. Orlando, W. D. Oliver, and S. Gustavsson, Phys. Rev. Lett. **114**, 010501 (2015).
- [54] D. Daems, A. Ruschhaupt, D. Sugny and S. Guérin, Phys. Rev. Lett. **111**, 050404 (2013).
- [55] S. Zeytinoğlu, M. Pechal, S. Berger, A. A. Abdumalikov Jr., A. Wallraff, and S. Filipp, Phys. Rev. A **91**, 043846 (2015).
- [56] A. Ruschhaupt, X. Chen, D. Alonso, and J. G. Muga, New J. Phys. **14**, 093040 (2012).
- [57] R. Barends, J. Kelly, A. Megrant, A. Veitia, D. Sank, E. Jeffrey, T. C. White, J. Mutus, A. G. Fowler, B. Campbell et al., Nature (London) **508**, 500 (2014).
- [58] J. F. Poyatos, J. I. Cirac, and P. Zoller, Phys. Rev. Lett. **78**, 390 (1997).
- [59] M. Reagor, C. B. Osborn, N. Tezak, A. Staley, G. Prawiroatmodjo, M. Scheer, N. Alidoust, E. A. Sete, N. Didier, M. P. da Silva et al., Sci. Adv. **4**, eaao3603 (2018).
- [60] S. A. Caldwell, N. Didier, C. A. Ryan, E. A. Sete, A. Hudson, P. Karalekas, R. Manenti, M. P. da Silva, R. Sinclair, E. Acala et al., Phys. Rev. Appl. **10**, 034050 (2018).
- [61] X. Li, Y. Ma, J. Han, T. Chen, Y. Xu, W. Cai, H. Wang, Y. P. Song, Z.-Y. Xue, Z.-Q. Yin, and L. Sun, Phys. Rev. Appl. **10**, 054009 (2018).
- [62] D. J. Egger, M. Ganzhorn, G. Salis, A. Fuhrer, P. Müller, P. K. Barkoutsos, N. Moll, I. Tavernelli, and S. Filipp, Phys. Rev. Appl. **11**, 014017 (2019).